applied sciences

MDPI

Article

Active Ankle–Foot Orthosis Design and Computer Simulation with Multi-Objective Parameter Optimization

Carlos Armando Lara-Velazquez [1], Juan-Pablo Ramirez-Paredes [1,*] and Beatriz Verónica González-Sandoval [2]

[1] Department of Electronics Engineering, University of Guanajuato, Carretera Salamanca—Valle de Santiago km 3.5 + 1.8, Comunidad de Palo Blanco, Salamanca 36787, Mexico; ca.laravelazquez@ugto.mx
[2] Department of Medicine and Nutrition, University of Guanajuato, Blvd. Milenio 1001, Predio San Carlos, León de los Aldama 37670, Mexico; bvgonzalez@ugto.mx
* Correspondence: jpi.ramirez@ugto.mx; Tel.: +52-464-647-9940

Abstract: There are many current active orthosis designs to assist with disabilities related to foot-drop, with most of them intervening during the whole gait cycle. We propose that, for the treatment of foot-drop, it is possible to design an ankle–foot device that will assist a walking user only during the dorsiflexion stages of the gait, avoiding interference with other stages, by using a single actuator with a simple transmission and a suspension block. This design can be improved by the use of multi-objective optimization to obtain a static set of parameters that are applicable to varying initial conditions. We present a computer simulation study of an active ankle–foot orthosis design, based on the interaction of a cam and lever with a suspension block, with the objective of assisting only with dorsiflexion during the gait cycle, leaving the rest of the movements unimpeded while reducing the complexity and weight of the device. This design is validated using a full simulation environment that includes the movements of the lower leg and foot, as they interact with our device and a ground element. As part of the design and validation, we found sets of mechanical and control parameters that provoke adequate output behavior of the orthosis to help the wearer perform a moderate-speed, normal gait. To optimize the design, we proposed three objectives to warrant ankle angle accuracy, minimal oscillations, and low energy consumption. A set of solutions was obtained with multi-objective optimization algorithms NSGA-II and RVEA to tune the parameters of the active orthosis. The solutions set from RVEA resulted in lower mean and standard deviation values for the oscillations and energy objectives in comparison to the solutions from NSGA-II, while for the MSE objective, NSGA-II obtained lower mean and standard deviation; for the energy consumption objective, the mean score using RVEA is 17% less than with NSGA-II. The orthosis is shown to be robust to differences in initial ankle angles. We observed that it is possible to obtain a broad set of solutions with a good performance during the gait cycle in controlled spaces and that in this application, the RVEA algorithm results in a better option for optimization to balance the objectives.

Keywords: multi-objective optimization; orthosis simulation; control optimization; assistive technology

check for updates

Citation: Lara-Velazquez, C.A.; Ramirez-Paredes, J.-P.; González-Sandoval, B.V. Active Ankle–Foot Orthosis Design and Computer Simulation with Multi-Objective Parameter Optimization. *Appl. Sci.* **2024**, *14*, 2726. https://doi.org/10.3390/app14072726

Academic Editor: Adel Razek

Received: 21 February 2024
Revised: 18 March 2024
Accepted: 21 March 2024
Published: 25 March 2024

Copyright: © 2024 by the authors. Licensee MDPI, Basel, Switzerland. This article is an open access article distributed under the terms and conditions of the Creative Commons Attribution (CC BY) license (https://creativecommons.org/licenses/by/4.0/).

1. Introduction

The gait altering condition known as "foot-drop" consists of the foot slapping down on the floor with each step and is generally caused by weakness of the foot and ankle dorsiflexor muscles. Foot-drop can cause falls and injuries [1], and its solutions can be conservative or nonconservative (surgical), which are generally avoided unless the gait impairment is severe [2]. A conservative solution that is very commonly used is an ankle–foot orthosis (AFO) [3] . Recently, researchers have worked on developing various technologies to enhance assistance and rehabilitation of foot-drop patients [4]. Functional electrical stimulation (FES) is another conservative solution studied and implemented by many authors [5]. However, Prenton et al. [6] concluded that AFOs have positive combined orthotic effects on walking that are equivalent to FES for foot-drop caused by stroke and

also found downsides of FES in the literature, including their complexity of setup, skin irritation, and pain.

Regarding AFO solutions, we can mention other orthosis devices for foot-drop, like the cable-driven wearable robots studied by Khomami and Najafi [7]. These devices are used more often as exoskeletons, and the authors concluded that cable-driven devices solve problems of excess weight and misalignment, having successfully addressed the issue of foot-drop. Moreover, end-effector-based robots have been used exclusively for rehabilitation purposes, and a significant disadvantage of this type of power transmission is that the amount of applicable shear force is limited by the comfort level of the wearer. Among the solutions presented with this technology, Kwon et al. [8] proposed a bidirectional tendon driven actuator to assist dorsiflexion and plantarflexion, where they presented successful results, but with limited validation. Technologies using electrical motors as actuators can be found in the literature; for instance, Yeung et al. [9] presented a lightweight but strong and wearable AFO with dorsiflexion assistance, weighing just 0.5 kg, reporting good results. This work does not mention a compliance element in the orthosis design, resulting in rigid actuation, which could be dangerous since external disturbances might damage the servomotor.

An important matter in the design of orthosis devices is their simulation by computers. The simulation of the gait cycle has been addressed and explored by different authors using various tools. For example, Eldirdiry et al. [10] simulated a robot foot in Simulink, where they proposed a platform to study human gait behavior, ensuring that it is possible to provide the main dynamic features of various cases of foot drop. Another standard software used for simulations and optimizations of orthosis devices is OpenSim, as in the case of Bermejo-Garcia et al. [11], who used dynamic optimization of anchor point positions in a cable-driven exosuit.

Three main complications must be solved in AFO design for foot-drop conditions: two of them are the slapping of the foot after the heel-strike (foot slap) and the dragging of the toe during the swing (toe drag) [12], and the third complication is ensuring that the natural push-off movement is not interrupted [13].

To address these challenges, we investigate the possibility of designing an ankle–foot device that will assist with walking only during the dorsiflexion stages of the gait, avoiding interference with other stages, and we propose that this design can be improved by the use of multi-objective optimization to obtain a static set of parameters that are applicable to varying initial conditions.

Hence, we present the design of a light, low-cost, and functional active AFO for foot-drop conditions. In addition, we simulate our device acting on a lower leg model with a foot-drop condition during the gait cycle, in a controlled environment, using the Multi-Joint Dynamics with Contact (MuJoCo) software, version 2.3.5. This simulation is used to address improvements and execute optimizations of the active AFO design parameters. The proposed simulation makes the design configurable through an optimization process.

Three objectives were proposed to warrant ankle angle accuracy, minimize oscillations, and reduce energy consumption. At the beginning of the study, we assumed that a user would achieve a gait pattern similar to a normal one after some time wearing the device. Like Arnez-Paniagua et al. [14], a database was used to obtain a reference signal to track the ankle angle. We apply two multi-objective optimization (MOO) algorithms to tune the parameters of two PD controllers and the mechanical properties of the suspensions. The sets of solutions obtained with each algorithm are compared to analyze their convergence and diversity.

To the best of our knowledge, this is the first time that a design, simulation, and multi-objective optimization of an active AFO have been developed. Our objective is to achieve a suitable design that avoids dragging, minimizes slapping, and does not affect push-off, while remaining low cost. The design has an electromechanical propulsion, a simple transmission, and two suspension elements controlled by a finite state machine. Our contributions are a novel AAFO design, aiming to enable the construction of a functional,

stable, and portable device that is also lightweight and low-cost; a system with small suspensions to create a compliant transmission, with a cam system for transmission of movement and easy escape; and a full simulation of tibia kinematics during a gait cycle to assess the AAFO design used in a multi-objective optimization scheme to obtain the best parameters for the orthosis depending on which objective is emphasized.

2. Materials and Methods

The simulation of a gait cycle for the design of an active AFO was implemented using MuJoCo [15]. In this work, the foot movement was restricted to a plane parallel to the sagittal plane, limiting it to flexion and dorsiflexion. We assume that when a patient is assisted with the AAFO, they should perform a normal ankle movement during the gait cycle. We used the database provided by Schreiber and Moissenet [16] with the kinematics and dynamics of the walking cycle of multiple healthy individuals at different speeds to obtain a reference lower leg movement. Our group has a prior AAFO design and simulation [17], upon which we built this work. As we will show, this new design improves the interaction between the moving parts and reduces backlash to the motor; the simulation is more complete and faithful due to the underlying software chosen for this work; and finally, the optimization is multi-objective according to three objective functions and performed using two different algorithms.

The orthosis design for modeling is depicted in Figure 1 and is explained in the following lines, with definitions for the most critical parts of the orthosis. Their control and synchronization are detailed in Section 2.1.

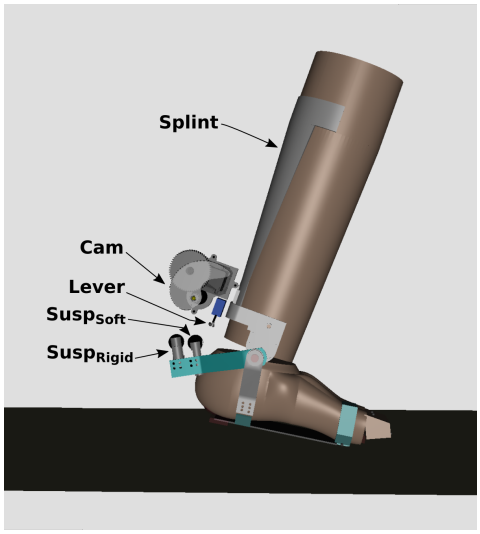

Figure 1. Model of the orthosis for simulation in MuJoCo. The main components are labeled.

Suspensions: A suspension system was designed for acting at different assistance stages, with two elements named $Susp_{Rigid}$ and $Susp_{Soft}$. The $Susp_{Rigid}$ element, composed of a spring and a shock absorber, will transfer movement from the cam to the ankle joint. It is rigid enough to preserve the position and to work as a compliant component for possible external disturbances, helping to protect the main servomotor. The element $Susp_{Soft}$, with just a spring component, has a low stiffness value and will contact the lever to reduce slapping.

Cam: This element provides two functions: transforming the circular movement of a motor into linear movement and having a simple escapement when it is inactive. This element is used to keep the AAFO motor from interfering with the later stages of the gait cycle. The cam makes contact with $Susp_{Rigid}$, and its profile has been designed to obtain a resolution of one degree per 0.2 mm of vertical displacement. Three functions were developed for the movement of this element during the gait cycle: Home-position, Follow-wheel, and Control.

Lever: This element has only two positions: home or active. The lever contacts $Susp_{soft}$ when active, according to the FSM. The purpose of this contact is used to avoid the foot slapping with the ground.

Servomotors: a Dynamixel MX106 servomotor was selected, and its torque and velocity were simulated by following the performance graph from the manufacturer. This actuator powers the movement of the cam. A smaller servomotor controls the lever element, enabling an opposition point to stop the $Susp_{Soft}$.

The servomotors were modeled after their specifications from the manufacturers, including their masses and moments of inertia. In the case of other components, the moments of inertia were computed by the simulator based on their geometries and material densities. The simulator was configured to use the Runge–Kutta 4th order solver, with a time step of 0.0001 s.

2.1. Control Description

We used a finite state machine (FSM), depicted in Figure 2, to control the AAFO during the different stages of the gait cycle. It consists of four states: Push-off, Swing, Swing-low, and Heel-strike. The simulation starts in the state Push-off of the FSM, just before starting the toe-off of the foot. Figure 3 depicts the stages of the FSM described during a gait cycle with the ankle angle reference signal. For a clearer FSM description, in the following lines, the inputs and outputs are explained, followed by the possible actions of the cam.

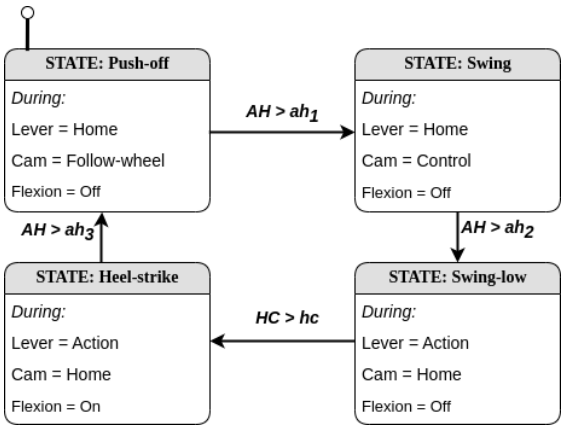

Figure 2. Finite state machine. Every block represents a state, and inside each block is the set of actions (value of outputs). AH and HC are the inputs, where AH is the ankle height, and HC is the heel contact, ah_1, ah_2, and ah_3 are the thresholds of ankle height, and hc is the threshold for the heel contact.

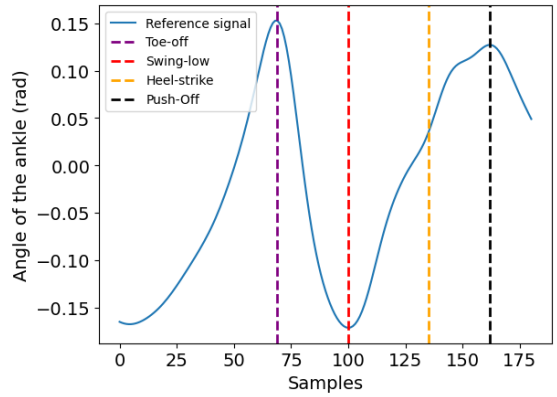

Figure 3. Ankle angle reference signal, with vertical lines indicating the starting points of every stage of the FSM. Toe-off is the start of the stage Swing, and other initial points have the name of its respective stage. The sampling rate is 0.01 s.

- Inputs: The height of the ankle and the heel contact were chosen as input signals. These ankle height thresholds (ah_1, ah_2, and ah_3) must be customized to the user. The heel contact with the ground hc is detected when the signal from a force sensor at the heel exceeds a minimum.
- Outputs: Movements of the cam, lever, and flexion of the ankle. The cam can perform three possible actions: Follow-wheel, Home-position, and Control. The Follow-wheel action consists of moving the cam and keeping its edge at a constant distance from the suspension, ensuring that any subsequent interactions between these elements are smooth. Otherwise, a strong contact may separate the elements instead of providing uniform pressure, thus affecting the Control action. The Home-position action is similar to Follow-wheel, but it increases the separation between the cam and suspension. During this action, no contact is expected to occur soon. Finally, the Control action follows the diagram of Figure 4, and it is explained in Section 2.2. During this action, the cam is in contact with the suspension. Given that the movement of the cam in the dorsiflexion direction demands more torque than in plantarflexion, a reduction factor of ten was applied when the ankle angle controller signal (Figure 4) results were negative, which means that the cam must move toward the plantarflexion direction.

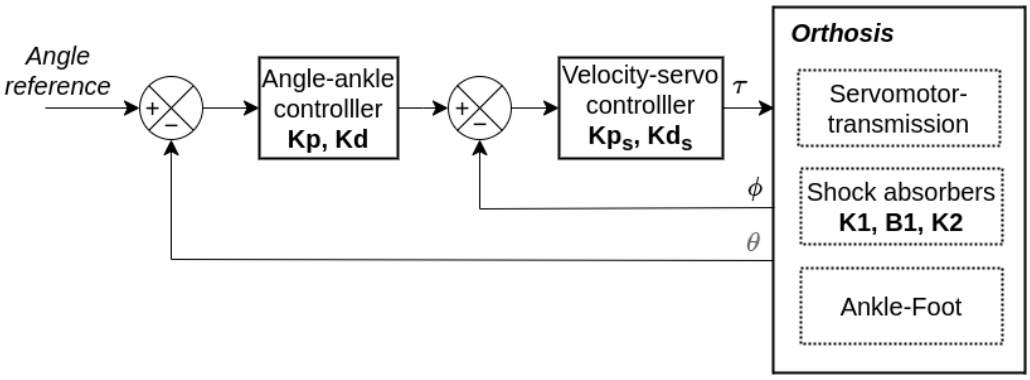

Figure 4. Control diagram applied during Swing state. The seven variables in bold are subjected to optimization in this work.

State Descriptions

- Push-off: This state keeps the lever inactive and the cam in Follow-wheel. In this part of the gait cycle, the user receives no assistance. The FSM passes from the last state to this once the input corresponding to the ankle height AH rises and exceeds the threshold ah_3, representing the user carrying all their weight with the other foot. In this state, the lever becomes inactive, and the ankle goes up freely until it exceeds the threshold ah_1, meaning the foot is about to take off from the ground.
- Swing: The next state starts in Toe-off (purple line in Figure 3). The lever remains inactive while the cam is enabled and controlled to apply dorsiflexion of the ankle to avoid dragging the foot.
- Swing low: This state, shown between the red and yellow vertical lines in Figure 3, is activated when the input AH goes below the threshold ah_2 and is completed once the Heel-strike starts. This state is an intermediate state, preparing for the Heel-strike, to allow the lever to be activated before $Susp_{Soft}$ raises an upper point. The cam is sent to the home position, consequently decreasing the dorsiflexion.
- Heel-strike: This last state, occurring between the yellow and black vertical lines in Figure 3, is activated once the input of the contact heel HC is higher than a threshold hc. In this stage of light resistance, a flexion torque is applied to the ankle joint of the simulated leg, emulating the AAFO user moving the foot down to the ground. Furthermore, the cam is kept at its home position, and the lever contacts $Susp_{Soft}$ to avoid slapping. This process reduces the energy consumption. In the last part of their stage, the $Susp_{Soft}$ releases a small amount of energy to reduce the human effort for

the loading response of the gait cycle. Finally, the gait cycle is completed, and the FSM switches to the Push-off state.

The angle of the ankle is estimated from three markers of the same person from the data of [16], and an offset is added to ensure that the foot remains free from drag during the Swing. This adjustment must be made because the calculation is an approximation of the ankle angle. In addition, exact measurements of the person's footwear are unavailable; consequently, the angle computed from the motion data may not be sufficient to free the toes from dragging.

2.2. Design Optimization and Control Tuning

2.2.1. Ankle Angle Control during Swing-State

A PD torque controller was applied to the transmission system during the Swing state to track the reference signal. Once this stage is finished, the lever element assists in the transition from Heel-strike to Push-up. Figure 4 shows the overall control scheme. The seven variables shown in the blocks are the design variables used to discover a set of values that minimize the three proposed objectives in Section 2.2.2. The signals ϕ, θ, and τ in the diagram correspond to the angular velocity of the cam, the angular position of the ankle, and the torque applied by the servomotor, respectively. We determined the decision space (range for every variable) that may result in an acceptable performance of the orthosis simulation during a gait cycle. The name, definition, and range for every variable are described in Table 1.

Table 1. Design variables for the AAFO optimization. All gains refer to controllers for the cam actuator. From the suspension block, the $Susp_{Rigid}$ element is a spring with a dampener, while $Susp_{Soft}$ is an element with just a spring.

Variable	Description	Min Value	Max Value
Kp	Proportional gain for external control	1	1×10^4
Kd	Derivative gain for external control	0	0.05
Kp_s	Proportional gain for internal control (Motor velocity)	0.005	0.1
Kd_s	Derivative gain for internal control (Motor velocity)	0	5×10^{-5}
$K1$	Stiffness of $Susp_{Rigid}$	5×10^3	5×10^4
$B1$	Damping of $Susp_{Rigid}$	0	20
$K2$	Stiffness of $Susp_{Soft}$	5	100

2.2.2. Objectives Definition

The optimization process was aimed to achieve good behavior and autonomy from the orthosis. Therefore, three objectives were selected to address ankle angle tracking accuracy, the amount of oscillations, and energy consumption. These objectives are as follows:

- MSE. The mean squared error between the ankle angle reference signal and the actual ankle angle is calculated to measure the ankle angle tracking accuracy.

$$\text{MSE} = \frac{1}{N}\sum_{n=1}^{N}(\theta_{out}(n) - \theta_{in}(n))^2 \quad (1)$$

  where N is the number of samples of the total simulation, $\theta_{out}(n)$ is the ankle angle output in radians at time sample n, and $\theta_{in}(n)$ is the ankle angle reference at time sample n. This $\theta_{in}(n)$ was set to 0 when the foot is 90 degrees relative to the tibia, with positive values for plantar flexion and negative values for dorsiflexion.
- Oscillations. The ankle angle signal must present a minimal amount of oscillations. This second objective was obtained with the following steps:

1. We determined that a Butterworth high-pass filter with a cut-off frequency of 10 and order 4 is adequate to separate the reference signal spectrum from unwanted components of the output.
2. After applying this filter, the power of the resulting signal is computed.

- Energy. The energy used for the servomotor should be minimized during the gait cycle to extend the AAFO use time. This objective is calculated from the integral of the power, computed as the product of the torque τ and the angular velocity ϕ.

$$E = \int_0^T \tau(t)\phi(t)dt \tag{2}$$

We decided to implement a flag to stop the simulation when the angle increases over 0.5 radians in flexion, which signals that the toes struck the floor. If the flag is activated, then the simulation ends and the costs of all objectives are set to their maximum. During optimization the variables are normalized in the range $[0, 1]$. In order to provide robustness to the solutions with respect to the initial dorsiflexion of the foot, we calculated the cost for every separate objective as the mean of 5 simulations with different initial positions of dorsiflexion from 7 to 13 degrees, i.e., with 1.5 degree increments.

2.2.3. Optimization Algorithm

The nature of these problems tends to have an underlying competition between objectives, so a multi-objective optimization (MOO) needed to be implemented to find a set of solutions rather than a unique best solution. The PYMOO library [18] was used to implement the MOO algorithms. The MOO algorithm Non-dominated Sorting Genetic Algorithm II (NSGA-II) [19] was chosen for the first testing, given its importance in many studies from the literature. A second optimization was implemented with the MOO algorithm Reference Vector Guided Evolutionary Algorithm (RVEA) [20]. This algorithm is mainly used for many-objective problems. The main new contributions in the RVEA lie in the two components: the reference vector-guided selection and the reference vector adaptation. This algorithm has a scaling approach termed the angle-penalized distance (APD), adopted to balance the convergence and diversity of the solutions in the high-dimensional objective space. The algorithm also has an adaptation strategy to dynamically adjust the reference vectors' distribution according to the scale of the objective functions.

3. Results

To illustrate the effect of using MOO algorithms to solve the parameter selection problem for our AAFO, we shall first show the performance of parameter sets chosen at random from Table 1. Five sets of parameters were generated from uniform distributions for each variable in the corresponding interval. We refer to this collection of parameter sets as 5-RS, and each parameter set is labeled from RS-0 to RS-4. Figure 5 shows the ankle angle output (left) and power output (right) resulting from the evaluation of 5-RS for one of the initial conditions (10 degrees of ankle angle). Note that parameter set RS-3, when evaluated in simulation, resulted in a tracking failure after around 100 time samples.

As Figure 5 shows, the performance of random sets of parameters is low and can even result in gross tracking errors. This introduces the need to apply some optimization procedure that ensures satisfactory performance of the AAFO. To this end, we configured our main simulation such that the parameters from Table 1 could be selected before execution, and the costs from Section 2.2.2 were obtained as outputs for each simulation run. We then used MOO algorithms to obtain solution sets that minimized the objectives. To ensure that the resulting solution sets consisted of parameters that provide certain robustness to varying initial conditions, in each simulation, the AAFO attempted to track the reference ankle angle signal five times, changing the initial ankle angle over a range of 7 to 13 degrees. Hence, the costs computed for each simulation run are actually the sum of those from the five tracking tasks.

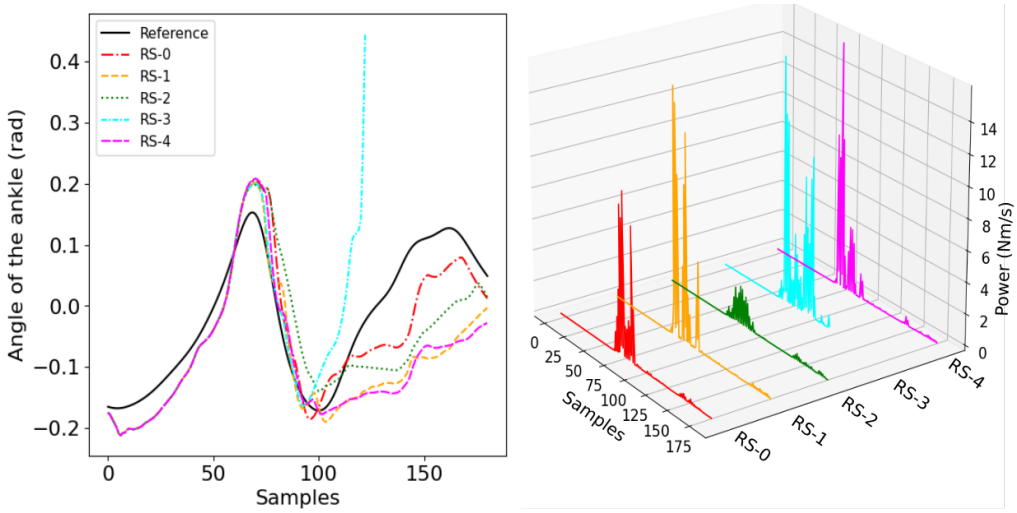

(**a**) Ankle angle outputs. (**b**) Power outputs.

Figure 5. Performance of some random sets of parameters, named RS-0 through RS-4, compared to a reference ankle angle signal. The (**a**) plot shows ankle angle output and the (**b**) plot power output, both with an initial condition of 10 degrees of ankle rotation. The plots for RS-3 end prematurely because that set of parameters causes the system to diverge.

The initial configuration for the NSGA-II implementation was set to 50 individuals and 300 generations, and for RVEA, we used 10 partitions and 300 generations. The search space for the MOO algorithms follows Table 1, and the objectives are those defined in Section 2.2.2. In this section, we will show the shape of the solution set, based on the costs for each objective, per individual in each MOO algorithm. Then, we will present the best solutions, according to each objective and for each MOO algorithm, both in a table and in graphs of ankle angle and energy expenditure. Some random parameter sets were also used to establish a baseline of performance, which will be compared to the solutions from the MOO algorithms to better illustrate their effectiveness in this application. Finally, we show the robustness of the solutions from the MOO algorithms under different initial conditions of the gait simulation.

3.1. Solution Sets from the MOO Algorithms

Figure 6 shows the set of solutions obtained by the NSGA-II algorithm (SS-NSGA-II) (Figure 6a) and the set of solutions obtained by the RVEA algorithm (SS-RVEA) (Figure 6b). It is possible to appreciate that NSGA-II preserves the initial population size, and all the elements in the set are non-dominated. Meanwhile, RVEA reduced the population from 65 (initial population for 10 reference vectors) to 44, and only 19 elements are non-dominated (red solutions in Figure 6b). Figures 7 and 8 show the different views of the SS-NSGA-II and SS-RVEA, respectively, in order to see with more detail the compromise between each pair of objectives.

Table 2 presents a list of the best solutions of SS-NSGA-II and SS-RVEA, from the perspective of every objective. The list contains the evaluation of the rest of the objectives and the set of parameters (solution selected). This table also shows the solution of every set that resulted in the best balance with regard to their respective means.

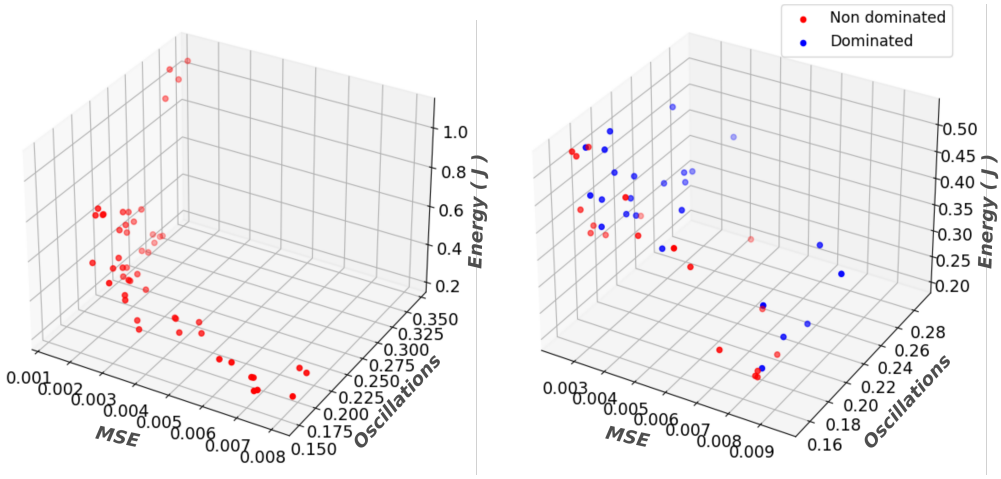

(**a**) NSGA-II set of solutions. (**b**) RVEA set of solutions.

Figure 6. Set of solutions from the optimization algorithms. The solutions from NSGA-II shown in (**a**) are all non-dominated. RVEA produced both dominated and non-dominated solutions, shown in (**b**) as red points and blue points, respectively.

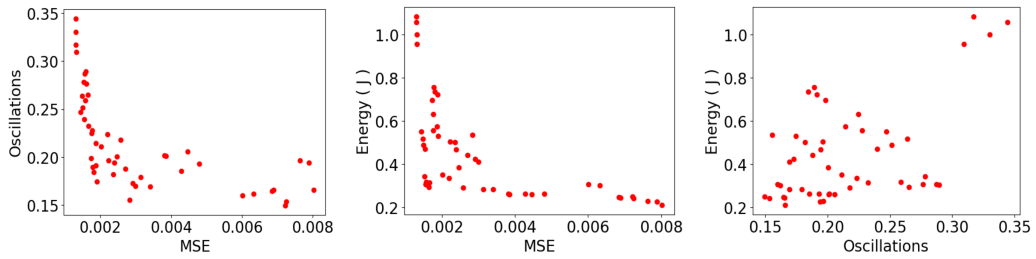

Figure 7. Planar views of the NSGA-II set of solutions, projecting them onto different combinations of two cost components. From left to right: MSE vs. Oscillations, MSE vs. Energy, and Oscillations vs. Energy.

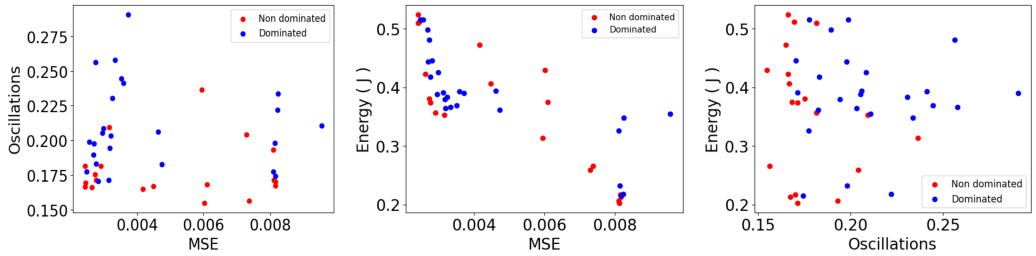

Figure 8. Planar views of the RVEA set of solutions, projecting them onto different combinations of two cost components. From left to right: MSE vs. Oscillations, MSE vs. Energy, and Oscillations vs. Energy.

Table 2. Best solutions by objective, for each optimization algorithm. The last row for each algorithm shows a balanced solution from its set, without emphasizing a single objective.

Element	Evaluations by Objective			Set of Parameters						
	MSE $\times 10^{-2}$	Osc.	Energy	Kp	Kd	Kp_s	Kd_s $\times 10^{-4}$	$K1$	$B1$	$K2$
NSGA-II										
Best MSE	0.1307	0.3173	1.0838	9479.7	0.0413	0.0222	0.2210	37121.0	6.350	47.864
Best osc.	0.7220	0.1494	0.2499	282.4	0.0273	0.0485	0.2006	25592.0	6.764	42.050
Best energy	0.8022	0.1658	0.2117	150.2	0.0438	0.1531	0.2436	23288.0	4.954	58.551
Balanced	0.2708	0.1877	0.4432	1943.7	0.0454	0.0097	0.0354	5099.0	15.454	12.201

Table 2. *Cont.*

Element	Evaluations by Objective			Set of Parameters						
	MSE $\times 10^{-2}$	Osc.	Energy	Kp	Kd	Kp_s	Kd_s $\times 10^{-4}$	$K1$	$B1$	$K2$
RVEA										
Best MSE	0.2422	0.1662	0.5241	1728.7	0.0315	0.0073	0.2027	30555.5	2.938	43.608
Best osc.	0.6021	0.1547	0.4294	1357.0	0.0336	0.0095	0.2069	30776.0	2.982	43.608
Best energy	0.8121	0.1713	0.2025	155.9	0.0065	0.1558	0.1771	30776.0	0.298	43.627
Balanced	0.4628	0.2060	0.3937	1360.9	0.0292	0.0100	0.1621	35658.5	2.320	44.263

3.2. Performance Evaluation of Selected Solutions

Figure 9 shows the response in the angle graph (left side) and power graph (right side), for one of the initial conditions (10 degrees of ankle dorsiflexion), of the solutions in Table 2 for SS-NSGA-II. Figure 10 shows the same information but for SS-RVEA. On the ankle angle response graph of both figures, the reference signal was added for clarity.

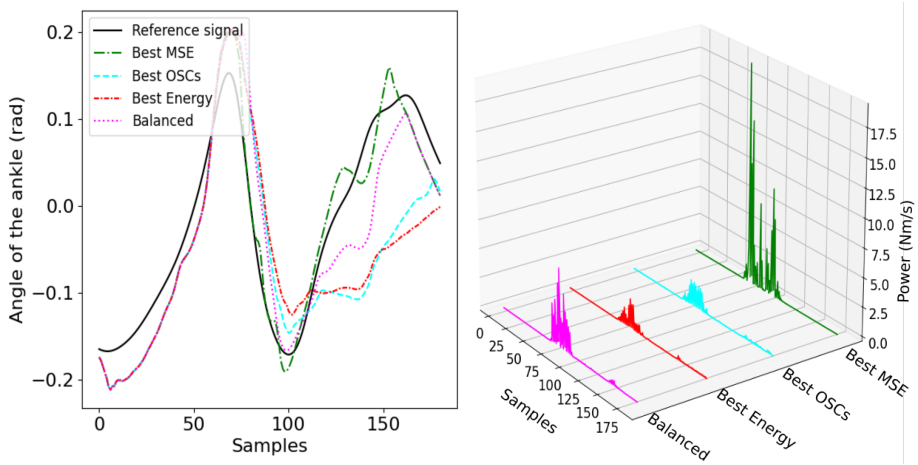

(**a**) Ankle angle outputs. (**b**) Power outputs.

Figure 9. Solutions from SS-NSGA-II that resulted in the best score regarding every objective, compared to the most balanced solution with respect to their mean. All the evaluations were initialized with an ankle angle of 10 degrees. Ankle angle output (**a**) and power output (**b**).

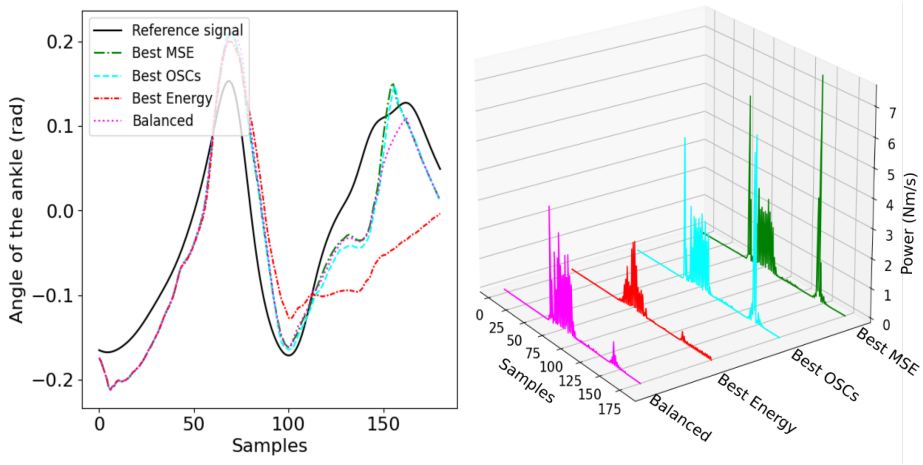

(**a**) Ankle angle outputs. (**b**) Power outputs.

Figure 10. Solutions from SS-RVEA that resulted in the best score regarding every objective, compared to the most balanced solution with respect to their mean. All the evaluations were initialized with an ankle angle of 10 degrees. Ankle angle output (**a**) and power output (**b**).

The mean μ and standard deviation σ by objective, for every set of solutions, is shown in Table 3, and the mean and standard deviation of 5-RS were added (excluding RS-3, which exceeded the angle limit).

Table 3. Mean and standard deviation of the the NSGA-II set of solutions, the RVEA set of solutions, and the random set of solutions (excluding RS-3).

Objective	Random		NSGA-II		RVEA	
	μ	σ	μ	σ	μ	σ
MSE	0.0072	0.0025	0.0031	0.0021	0.0047	0.0023
Oscillations	0.3104	0.058	0.2150	0.0490	0.1954	0.0307
Energy	0.6640	0.2531	0.4465	0.2244	0.3728	0.0918

In order to appreciate the robustness of the solutions to the initial ankle angle, Figure 11 shows the ankle angle signal and the power signal resulting from simulating the best individual, chosen by MSE objective from the SS-NSGA-II, at the different initial conditions (from 7 to 13 degrees). Figure 12 shows the same cases for SS-RVEA.

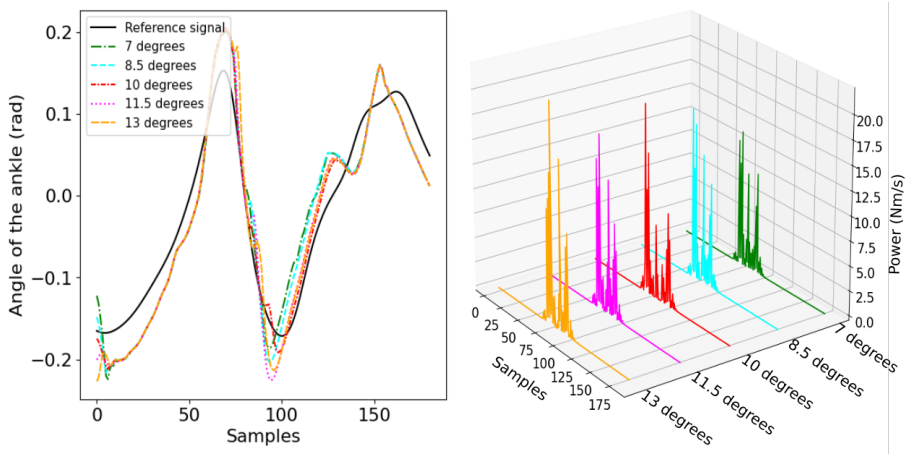

(**a**) Ankle angle outputs. (**b**) Power outputs.

Figure 11. NSGA-II. Robustness to different initial ankle angles during the gait cycle, for the best MSE solution. Plot (**a**) is the ankle angle output over time, and (**b**) is the power output over time, for each initial condition in ankle angle.

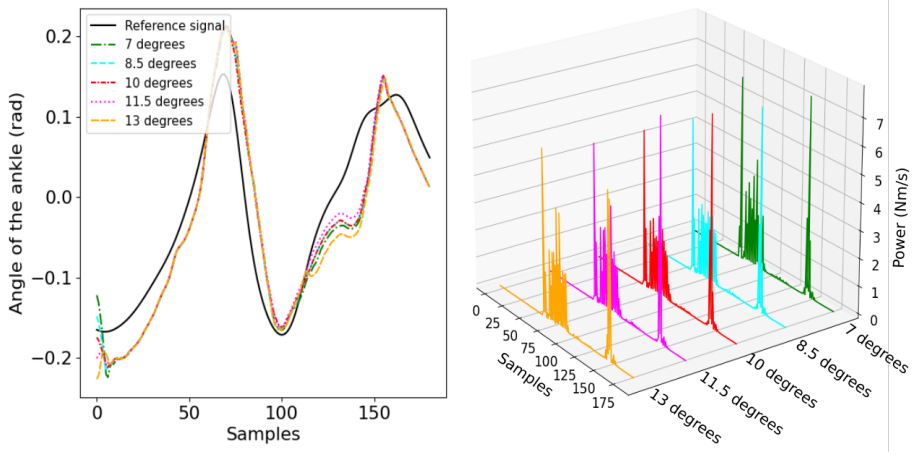

(**a**) Ankle angle outputs. (**b**) Power outputs.

Figure 12. RVEA. Robustness to different initial ankle angles during the gait cycle, for the best MSE solution. Plot (**a**) is the ankle angle output over time, and (**b**) is the power output over time, for each initial condition in ankle angle.

4. Discussion

Figures of the 2D views of the set of solutions show evidence of the compromise between the different objectives since they all present a Pareto-front shape curve. Regarding robustness to the initial ankle angle, using the best solution with respect to the MSE for both MOO algorithms, we appreciated low variations, a fact which demonstrates that the system can quickly recover its position and that the performance is not affected at all during the rest of the gait cycle. As both sets of solutions show the same, we can assure robustness for initial dorsiflexion of the ankle in a range of 7 to 13 degrees.

The parameter sets from 5 to RS produced one set with costs out of limits, and the rest of them had mean costs and standard deviations clearly worse than the solutions from SS-NSGA-II and SS-RVEA. We determined that on the established decision space, we can likely find moderate performance solutions even with short optimizations. With random selection, we would obtain parameters that surely will not even be close to the Pareto-front, and therefore optimization is necessary.

After 300 generations, SS-RVEA resulted in 19 non-dominated solutions and 25 dominated, while SS-NSGA-II resulted in all the solutions being non-dominated. We could resume the comparison of mean and standard deviation among SS-NSGA-II and SS-RVEA as follows: for the MSE objective, values from SS-NSGA-II resulted better than the ones from SS-RVEA, but for the oscillations and energy objectives, SS-RVEA values resulted better than SS-NSGA-II values, with a more notable difference in the third objective, where the mean from SS-RVEA is 17% less than the mean from SS-NSGA-II.

While both MOO algorithms produced varied sets of valid solutions, it is possible to observe a better balance between objectives in solutions of SS-RVEA. In contrast, SS-NSGA-II solutions tend to charge toward some objective, and therefore, the best-scored solution by MSE objective results in the worst score by other objectives.

The present AAFO design and simulation can be used with many different operating conditions, thanks to the underlying MuJoCo engine. Other simulation efforts are mainly based on the OpenSim platform (e.g., [21]), which is very useful to obtain inverse kinematics and inverse dynamics from human motion capture data, but it is not simple to modify to emulate orthoses and exoskeletons. Unlike prior efforts that apply transfer function identification to tune a PID controller for an ankle actuator at different gait stages [10], we apply multi-objective optimization to find a set of gains that are applicable to the whole gait cycle.

Some works have proposed to simulate exoskeletons as direct torques applied to the joints of a musculoskeletal model, like [22,23], but assume that the actuators are massless. Our work considers masses and actuation limits that follow the specifications from a manufacturer, unlike other efforts that assume that torques are instantaneous [24].

As for limitations of our proposed AAFO, we shall mention that the control strategy, both at the actuator level and at the FSM, is not considering walking motions over different surfaces, so at this moment, it is focused on restoring normal gait only on flat and even ground.

Based on the results from this study, the next phase of this research will be the implementation of the AAFO design as a real prototype, using materials with mechanical properties close to their simulated counterparts and using the proposed servomotors, so that validating experiments can be conducted on a test bench.

5. Conclusions

This work presents a complete design and simulation of an untethered, light, and low-cost active ankle–foot orthosis (AAFO), aimed at assisting persons with ailments resulting in foot-drop, but which does not interfere in the plantar flexion process. Unlike other designs in the literature requiring variable impedance for the joint, this work implements a cam in series with a compliant element system transmission. The MuJoCo engine allowed us to obtain great flexibility and accuracy in simulation. Using reference gait patterns for

the lower leg, we design and control the AAFO-corrected foot-drop in our simulation tests, even under varying initial conditions of the foot and ankle.

We chose three performance objectives for the AAFO optimization: mean squared error with respect to a reference ankle angle signal, smoothness of the same signal, and the amount of energy used by the servomotor. The multi-objective optimization strategies NSGA-II and RVEA provided results that tend to favor RVEA as a better source of solutions, since they are less clustered in the cost function space. For this design, MOO algorithms made it possible to obtain a broad set of solutions with good performance during the gait cycle in controlled conditions, and the RVEA algorithm provided a better diversity of solutions.

Author Contributions: Conceptualization, C.A.L.-V., B.V.G.-S. and J.-P.R.-P.; software, C.A.L.-V.; methodology, J.-P.R.-P.; investigation, C.A.L.-V. and B.V.G.-S.; validation, C.A.L.-V.; writing—original draft preparation, C.A.L.-V.; writing—review and editing, J.-P.R.-P.; supervision, J.-P.R.-P.; project administration, J.-P.R.-P.; funding acquisition, J.-P.R.-P. and B.V.G.-S.; resources, J.-P.R.-P. and B.V.G.-S. All authors have read and agreed to the published version of the manuscript.

Funding: This research was funded by the Innovation, Science and Entrepreneurship Institute for Competitiveness of Guanajuato State (IDEA GTO), under grant number IDEAGTO/CONV/033/2022. Author C.A.L.V. thanks the Mexican Council for Humanities, Science and Technology (CONAHCYT) for graduate fellowship 662285.

Institutional Review Board Statement: Not applicable.

Informed Consent Statement: Not applicable.

Data Availability Statement: The data presented in this study are available on request from the corresponding author.

Conflicts of Interest: The authors declare no conflicts of interest. The funders had no role in the design of the study; in the collection, analyses, or interpretation of data; in the writing of the manuscript; or in the decision to publish the results.

Abbreviations

The following abbreviations are used in this manuscript:

AAFO	Active ankle–foot orthosis
MOO	Multi-objective optimization
FSM	Finite state machine
MSE	Mean squared error
FES	Functional electrical stimulation
NSGA-II	Non-dominated Sorting Genetic Algorithm II
RVEA	Reference Vector Guided Evolutionary Algorithm
SS-NSGA-II	Set of solutions resulting from the optimization using the NSGA-II algorithm
SS-RVEA	Set of solutions resulting from the optimization using the RVEA algorithm

References

1. Stewart, J.D. Foot drop: Where, why and what to do? *Pract. Neurol.* **2008**, *8*, 158–169. [CrossRef] [PubMed]
2. Nori, S.L.; Stretanski, M.F. Foot Drop. In *StatPearls*; StatPearls Publishing: Treasure Island, FL, USA, 2022.
3. Chin, R.; Hsiao-Wecksler, E.T.; Loth, E.; Kogler, G.; Manwaring, S.D.; Tyson, S.N.; Shorter, K.A.; Gilmer, J.N. A pneumatic power harvesting ankle-foot orthosis to prevent foot-drop. *J. NeuroEng. Rehabil.* **2009**, *11*, 19. [CrossRef] [PubMed]
4. Alnajjar, F.; Zaier, R.; Khalid, S.; Gochoo, M. Trends and Technologies in Rehabilitation of Foot Drop: A Systematic Review. *Expert Rev. Med. Devices* **2021**, *18*, 31–46. [CrossRef] [PubMed]
5. Sabut, S.K.; Bhattacharya, S.D.; Manjunatha, .M. Functional Electrical Stimulation on Improving Foot Drop Gait in Poststroke Rehabilitation: A Review of its Technology and Clinical Efficacy. *Crit. Rev. Biomed. Eng.* **2013**, *41*, 149–160. [CrossRef] [PubMed]
6. Prenton, S.; Hollands, K.; Kenney, L.P. Functional electrical stimulation versus ankle foot orthoses for foot-drop: A meta-analysis of orthotic effects. *J. Rehabil. Med.* **2016**, *48*, 646–656. [CrossRef] [PubMed]
7. Khomami, A.M.; Najafi, F. A survey on soft lower limb cable-driven wearable robots without rigid links and joints. *Robot. Auton. Syst.* **2021**, *144*, 103846. [CrossRef]

8. Kwon, J.; Park, J.H.; Ku, S.; Jeong, Y.H.; Paik, N.J.; Park, Y.L. A Soft Wearable Robotic Ankle-Foot-Orthosis for Post-Stroke Patients. *IEEE Robot. Autom. Lett.* **2019**, *4*, 2547–2552. [CrossRef]
9. Yeung, L.F.; Ockenfeld, C.; Pang, M.K.; Wai, H.W.; Soo, O.Y.; Li, S.W.; Tong, K.Y. Randomized controlled trial of robot-assisted gait training with dorsiflexion assistance on chronic stroke patients wearing ankle-foot-orthosis. *J. NeuroEng. Rehabil.* **2018**, *15*, 51. [CrossRef] [PubMed]
10. Eldirdiry, O.; Zaier, R.; Al-Yahmedi, A.; Bahadur, I.; Alnajjar, F. Modeling of a biped robot for investigating foot drop using MATLAB/Simulink. *Simul. Model. Pract. Theory* **2020**, *98*, 101972. [CrossRef]
11. Bermejo-García, J.; Jorge, D.R.; Romero-Sánchez, F.; Alonso, F.J. Dynamic optimization of anchor points positions in a cable driven exosuit: A computer simulation approach. *Mech. Based Des. Struct. Mach.* **2023**. [CrossRef]
12. Blaya, J.A.; Herr, H. Adaptive Control of a Variable-Impedance Ankle-Foot Orthosis to Assist Drop-Foot Gait. *IEEE Trans. Neural Syst. Rehabil. Eng.* **2004**, *12*, 24–31. [CrossRef] [PubMed]
13. Shorter, K.A.; Xia, J.; Hsiao-Wecksler, E.T.; Durfee, W.K.; Kogler, G.F. Technologies for Powered Ankle-Foot Orthotic Systems: Possibilities and Challenges. *IEEE/ASME Trans. Mechatronics* **2013**, *18*, 337–347. [CrossRef]
14. Arnez-Paniagua, V.; Rifaï, H.; Amirat, Y.; Mohammed, S. Adaptive control of an actuated-ankle-foot-orthosis. In Proceedings of the IEEE International Conference on Rehabilitation Robotics, London, UK, 17–20 July 2017; pp. 1584–1589. [CrossRef]
15. Todorov, E.; Erez, T.; Tassa, Y. MuJoCo: A physics engine for model-based control. In Proceedings of the 2012 IEEE/RSJ International Conference on Intelligent Robots and Systems, Vilamoura-Algarve, Portugal, 7–12 October 2012; pp. 5026–5033. [CrossRef]
16. Schreiber, C.; Moissenet, F. A multimodal dataset of human gait at different walking speeds established on injury-free adult participants. *Sci. Data* **2019**, *6*, 111. [CrossRef] [PubMed]
17. Lara-Velazquez, C.A.; Ramirez-Paredes, J.P.; Martinez-Ramirez, I.; Nunez-Altamirano, D.A.; Gonzalez-Sandoval, B.V.; Torres-Del-Carmen, F.; Correa-Tome, F.E.; Perez-Ramirez, L.E.; Velazquez-Bustamante, A.E. Design and Simulation of an Active Ankle-Foot Orthosis with Parameter Optimization. In Proceedings of the 2022 International Conference on Mechatronics, Electronics and Automotive Engineering (ICMEAE), Cuernavaca, Mexico, 5–9 December 2022; pp. 7–12. [CrossRef]
18. Blank, J.; Deb, K. pymoo: Multi-Objective Optimization in Python. *IEEE Access* **2020**, *8*, 89497–89509. [CrossRef]
19. Deb, K.; Pratap, A.; Agarwal, S.; Meyarivan, T. A fast and elitist multiobjective genetic algorithm: NSGA-II. *IEEE Trans. Evol. Comput.* **2002**, *6*, 182–197. [CrossRef]
20. Cheng, R.; Jin, Y.; Olhofer, M.; Sendhoff, B. A Reference Vector Guided Evolutionary Algorithm for Many-Objective Optimization. *IEEE Trans. Evol. Comput.* **2016**, *20*, 773–791. [CrossRef]
21. Fournier, B.N.; Lemaire, E.D.; Smith, A.J.J.; Doumit, M. Modeling and Simulation of a Lower Extremity Powered Exoskeleton. *IEEE Trans. Neural Syst. Rehabil. Eng.* **2018**, *26*, 1596–1603. [CrossRef] [PubMed]
22. Bianco, N.A.; Franks, P.W.; Hicks, J.L.; Delp, S.L. Coupled Exoskeleton Assistance Simplifies Control and Maintains Metabolic Benefits: A Simulation Study. *PLoS ONE* **2022**, *17*, e0261318. [CrossRef] [PubMed]
23. Bianco, N.A.; Collins, S.H.; Liu, K.; Delp, S.L. Simulating the Effect of Ankle Plantarflexion and Inversion-Eversion Exoskeleton Torques on Center of Mass Kinematics during Walking. *PLoS Comput. Biol.* **2023**, *19*, e1010712. [CrossRef] [PubMed]
24. Nguyen, V.Q.; Umberger, B.R.; Sup, F.C. Predictive Simulation of Human Walking Augmented by a Powered Ankle Exoskeleton. In Proceedings of the 2019 IEEE 16th International Conference on Rehabilitation Robotics (ICORR), Toronto, ON, Canada, 24–28 June 2019; pp. 53–58. [CrossRef]

Disclaimer/Publisher's Note: The statements, opinions and data contained in all publications are solely those of the individual author(s) and contributor(s) and not of MDPI and/or the editor(s). MDPI and/or the editor(s) disclaim responsibility for any injury to people or property resulting from any ideas, methods, instructions or products referred to in the content.